Laser powder bed fusion of porous graded structures: A comparison between computational and experimental analysis

Sergio Ruiz de Galarreta [a],[*], Ruben J. Doyle [b], Jonathan Jeffers [b], Shaaz Ghouse [b]

[a] Department of Mechanical Engineering and Materials, Universidad de Navarra, TECNUN Escuela de Ingenieros, Paseo Manuel de Lardizabal, 13, 20018, San Sebastian, Spain
[b] Department of Mechanical Engineering, Imperial College London, London, SW7 2AZ, United Kingdom

ARTICLE INFO

ABSTRACT

Functionally graded porous structures (FGPSs) are gaining interest in the biomedical sector, specifically for orthopaedic implants. In this study, the compressive behaviour of seven different FGPSs comprised of Face Centred Cubic (FCC) and the Octet truss unit cells (OCT) were analysed. The porosity of the structures were graded in different directions (radially, longitudinally, laterally and longitudinally & radially) by varying the strut diameters or by combining the two types of unit cells. The structures were manufactured by laser power bed fusion and compression tests were performed. Radially and laterally porous graded structures were found to outperform uniform porous structures with an increase in stiffness of 13.7% and 21.1% respectively. The experimental and finite element analysis (FEA) results were in good agreement with differences in elastic modulus of 9.4% and yield strength of 15.8%. A new FEA beam model is proposed in this study to analyse this type of structures with accurate results and the consequent reduction of computational time. The accuracy of the Kelvin-Voight model and the rule of mixtures for predicting the mechanical behaviour of different FGPSs was also investigated. The results demonstrate the adequacy of the analytical models specifically for hybrid structures and for structures with smooth diameter transitions.

1. Introduction

Developments in Additive Manufacturing (AM) have led to an increased interest in structures that cannot be conventionally machined, such as lattice structures. Lattice structures also known as cellular or porous structures are a type of material comprised of a stochastic (random) or periodic framework of beams (struts). These structures can also consist of struts or surfaces represented by mathematical equations, e.g. triply periodic minimal surfaces (TPMS). The mechanical properties of these structures are governed by the parent material, the architecture of the unit cell/structure and the size and porosity of the unit cell/structure. The properties of these lightweight structures make them ideal for scaffolds (Blázquez-Carmona et al., 2021) and medical implants such as hip (Jetté et al., 2018) or dental implants (Wally et al., 2019).

In addition to uniform or periodic unit cell lattice structures, which are commonly studied in the literature (Hedayati et al., 2016; Herrera et al., 2014), functionally porous graded structures (FPGSs) are of great interest. These structures which gradually change the porosity and/or stiffness or strength throughout the component may improve bone

ingrowth and implant fixation (Ghouse et al., 2019; Han et al., 2018). A common way to design FGPSs is to gradually increase or decrease the strut diameter (for strut-based lattice structures) (Limmahakhun et al., 2017a; Maskery et al., 2016; Mahbod and Asgari, 2019) or the surface thickness (for TPMS) (Zhou et al., 2020; Zhao et al., 2020; Yang et al., 2019). Scaling the unit cell size in specific directions is also used to vary the porosity of these structures (Al-Ketan et al., 2020; Liu et al., 2018a), however this method offers limited variation. Alternatively the porosity of the structures can be varied by combining different types of unit cells (Al-Ketan et al., 2020; Maskery et al., 2018). However, depending on the type of unit cells a mismatch of struts can occur at unit cell boundaries and therefore the range of unit cells that could be used for this hybridization is also limited.

The quasi-static behaviour of radially graded porous structures (Xiong et al., 2020; Limmahakhun et al., 2017b; Montazerian et al., 2019; Zhang et al., 2019), axially graded porous structures (Mahbod and Asgari, 2019; Zhao et al., 2020; Maskery et al., 2018; Wang et al., 2019; Liu et al., 2018b) and laterally graded porous structures (Yang et al., 2019) has previously been reported. To predict the behaviour of the

* Corresponding author.
E-mail address: sruiz@tecnun.es (S. Ruiz de Galarreta).

metal FGPSs, some studies use finite element analysis (FEA), with structures being modelled in different ways. Zhang et al. (2019) studied diamond strut-based FGPS by analysing a representative volume element (RVE) and incorporating manufacturing geometric imperfections. With the defect-couple RVE model, they found very low differences (~2%) between the FEA results and the experiments for radially porous graded structures. Yang et al. (2019) analysed FGPSs (axially and laterally graded porous structures) made by gyroid TPMS assuming no geometric and material imperfections inherent to the manufacturing process. They found that the porosity gradient perpendicular to the direction of loading, increases the Young's modulus and yield strength of the cellular structures. However, these values were not compared between FEA and experiments. Working with polymers, Mahbod and Asgari (2019) modelled FGPSs (axially graded) made by double pyramid dodecahedron unit cells with Timoshenko beam elements and developed an analytical model. The errors with the experiments were relatively low (~10%). Bai et al. (2020) analysed the energy absorption and mechanical properties of porous graded nylon structures, in this study the density of the structures was varied by altering the unit cell height. Some studies also use the Kelvin-Voight-model and the rule of mixtures to analytically predict the elastic modulus and yield strength of axially (Maskery et al., 2018), radially and laterally (Yang et al., 2019; Zhang et al., 2019) graded porous structures. Usually the difference between these models and FEA is greater for axially porous graded structures where the Kelvin-Voight-model is used and the difference ranges from 3% to 20% (Maskery et al., 2018). For radially and laterally graded porous structures the error is lower and ranges from 1% to 12% (Yang et al., 2019; Zhang et al., 2019).

The main purpose of this work is to propose and to verify numerical procedures that can accurately model any FGPS structure independently of the grading direction. It should be noted that most of the studies in the literature employing FEA to model FGPSs use the explicit solver in the numerical simulations in order to account for the big deformations and the contact between struts. The advantage of this procedure is that the energy absorption of the structures can be numerically predicted. However, as shown in the literature, in general, this procedure is not so accurate when analysing the elastic properties of FGPSs (elastic modulus and yield strength). Considering that in many applications the FGPSs will work in the elastic region, it is necessary to define a numerical procedure that can represent them accurately. To this end, in this work the yield strength and elastic modulus of different FGPSs are numerically analysed and compared to the experiments. The structures analysed in this work are formed by the modified Faced-Centred-Cubic (FCC) and Octet truss (OCT) unit cells. In order to check the validity of these procedures for different FGPSs, the porosity was graded in different directions: radially, axially, laterally and mixed (axially & radially), by varying the strut diameters and by combining the two types of unit cells. The first step was to analyse the adequacy of analytical models (Kelvin-Voight model and the rule of mixtures) analysing 46 different porous graded structures and comparing the analytical results with the FEA results. Then, seven different type of FGPSs were designed, manufactured and compression tested to obtain the mechanical properties. These structures were also computationally analysed by the procedure described by Ruiz de Galarreta et al. (Ruiz de Galarreta et al., 2020), by a new FEA procedure using beam elements and by analytical models.

2. Materials and methods

In section 2.1 the design of the seven different porous-graded structures that will be experimentally and numerically analysed is described. Section 2.2 describes the analytical models defining the behaviour of FGPSs. To check the adequacy of these models for different FGPSs, 46 structures with different strut diameters, porosity gradients and unit cell sizes (1.5 and 2.5 mm) are studied. In section 2.3, the different FEA procedures analysed in this work are detailed. And finally,

in section 2.4 the fabrication of the samples and the compressive tests are described. A scheme of the different analysis is illustrated in Fig. 1.

2.1. Design of structures

Seven different types of porous-graded structures were studied in this work. PTC CREO 5.0 (PTC Inc.) was used to design the structures, comprised of either a modified Face-Centred-Cubic (FCC) unit cell, an Octet truss (OCT) unit cell, as described in literature (Ruiz de Galarreta et al., 2020), or a combination of the two. The unit cell size for all the structures is 1.5 mm and all the structures are formed by $10 \times 10 \times 15$ unit cells ($15 \times 15 \times 22.5$ mm); 10 unit cells in the width directions (X and Z axes) and 15 unit cells in the height direction (Y axis). These structures are divided in different regions/layers depending on the porous gradient. The porous-graded lattice structures are described below and illustrated in Fig. 2:

- A longitudinally porous graded FCC structure where the diameter of the struts decreases from the top to the bottom. In this structure, five different regions with their own specific strut diameter were defined (Fig. 2-a). Each region (or layer) will be formed by $10 \times 10 \times 3$ unit cells. This structure will be denoted in this work as *LG*.
- A laterally porous graded FCC structure where the diameter of the struts varies in the X-direction with five different regions (Fig. 2-b). Each region (or layer) will be formed by $2 \times 10 \times 15$ unit cells. This structure will be denoted in this work as *LTG*.
- Two radially porous graded FCC structures where the diameters vary in the radial direction. In the first structure, the maximum diameter is in the outside, while in the second structure it is in the inside of the structure. Again, five different regions were defined (Fig. 2-c). These structures will be denoted in this work as *RG1 & RG2*. In the figure, the top view of the RG1 structure is displayed, front view is not displayed as there is no porous gradient in the height direction (Y axis).
- A longitudinally and radially FCC graded structure, where the strut diameters vary both longitudinal and radially. In the longitudinal direction three different regions were defined and each region was radially graded as illustrated in Fig. 2-e. This structure will be denoted in this work as *LRG*. Both top and front views of this structure are displayed in the figure.
- The last two porous-graded structures are a radially porous graded structure and a laterally porous graded structure. However, in this case the porosity was varied not by changing the strut diameter, but by combining two different unit cells, the FCC and the Octet-truss unit cells. These structures will be denoted in this work as *MRG & MLTG*. For the MRG structure the two outer layers are formed by OCT unit cells, and the three inner layers by the FCC unit cells (Fig. 2-d). In the figure, the top view of this structure is displayed. For the MLTG structure, half of the structure is composed by FCC unit cells and the other half by OCT unit cells, i.e. $5 \times 10 \times 15$ FCC unit cells and $5 \times 10 \times 15$ OCT unit cells.

The procedure to determine the corresponding strut diameter for each of the layers of the structure is explained in Section 2.4.2 and the values are displayed in section 3.2.

2.2. Analytical models

Prior to simulating the mechanical behaviour of the designed structures, preliminary work analysed analytical models utilised previously in literature. The accuracy estimating the stiffness of porous graded structures of the Kelvin-Voight model (Eq. (1)) and the rule of mixtures for composite materials (Eq. (2)) were analysed by studying four types of graded porous structures: longitudinally, radially and laterally porous graded FCC structures; and a radially graded structure formed by the FCC and OCT unit cells. For each type of structure, at least
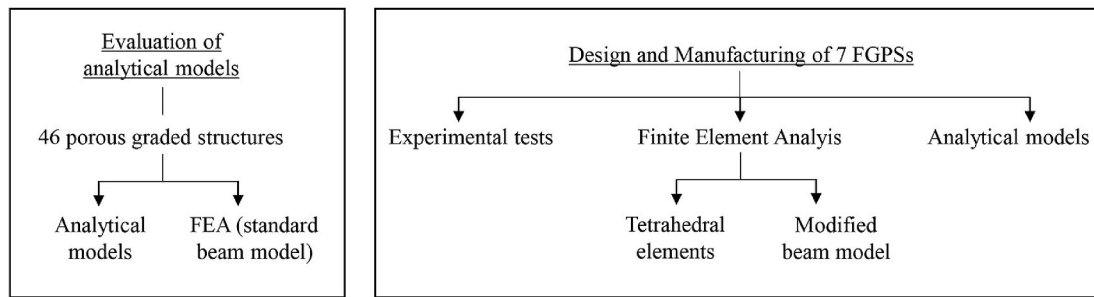
Fig. 1. Diagram of the different analysis of the FGPSs.

10 different specimens with different diameters and porosity gradients were analysed. All the structures were composed by $10 \times 10 \times 15$ unit cells, and two different sizes of unit cell (1.5 mm and 2.5 mm) were used.

$$\frac{1}{E} = \sum_{i=1}^{n} k_i \frac{1}{E_i} \tag{1}$$

$$E = \sum_{i=1}^{n} k_i E_i \tag{2}$$

In these equations, n denotes the total number of layers (in the longitudinal or radial direction), k_i is the volume percentage of the corresponding layer with respect to the entire lattice structure, E the initial elastic modulus of the graded structure and E_i the elastic modulus corresponding to layer i, which depends on its relative density. To this end, the Gibson and Ashby model (Eq. (3)) (Gibson and Ashby, 1997; Ashby, 2006), which describes the elastic modulus (E) of a lattice as a function of its relative density, was derived for the FCC and OCT lattice structures.

$$\frac{E}{E_0} = C \left(\frac{\rho}{\rho_0} \right)^m \tag{3}$$

where E_0 and ρ_0 are the base material properties and C and m are constants that should be determined for each of the structures (FCC and OCT). The methodology to analytically estimate the stiffness of the graded structures was as follows: first calculate the relative density for each layer, then calculate the stiffness of the corresponding layer by using Equation (3) and finally obtain the stiffness of the graded structures by utilising Equation (1) or 2 depending on whether it is a longitudinal graded porous structure or a radial/lateral porous graded structure.

The results for the 46 structures were then compared to FEA results to check the adequacy of the analytical models. The coefficients for Equation (3) where derived in section 2.3.1.

The initial elastic modulus and yield strength of the seven FGPSs described in section 2.1 were also calculated analytically using equations (1) and (2) and the Gibson and Ashby curves obtained in (Ruiz de Galarreta et al., 2020). As mentioned above Equation (1) was used for the LG structure, while Equation (2) was used for the RG, LTG, MRG and MLTG structures. For the LRG structure both equations were used. Firstly, Equation (2) was used to determine the modulus of each longitudinal layer, and then Equation (1) was used to calculate the elastic modulus of the structure.

2.3. Finite element analysis

In this section, the three different FEA procedures followed in this work are described. The first one is the most simple and it was only used to analyse the adequacy of the analytical models (with the 46 porous graded structures that can be found in the supplementary material). The second and third one were applied to the seven FGPSs described in section 2.1. The three procedures are based on a methodology described

previously (Ruiz de Galarreta et al., 2020). ABAQUS 2020 (Dassault Systems) was used for numerical simulations. Compression platens were simulated by modelling two rigid shells (meshed with rigid rectangular elements R3D4) with a reference point. The bottom shell was encastred and all the degrees of freedom, except the displacement in the compression direction, were constrained for the top shell. The displacement applied to the top shell was set to progressively deform the FGPSs until they yield, with macroscopic strains ranging from 1% to 2% depending on the FGPS. Table 1 displays the bilinear elasto-plastic material model used for all the structures which was previously derived from uniaxial tensile tests of stainless steel struts with different diameters, in the same range as in this work.

From the FE results, engineering stress – strain curves were generated and the linear initial loading portion of the stress – strain curves was used to determine the modulus of the structures. Yield strength was taken at a 0.2% strain offset. Stress was defined as the reaction force on the rigid shells at the reference point divided by the specimen cross-sectional area (using the macro/apparent dimensions). The vertical displacement of the top shell divided by the original height of the structure was used to calculate strain.

2.3.1. Numerical modelling of porous graded structures with standard beam model

This procedure was followed to study the adequacy of the analytical models and it was applied to the 46 porous graded structures described in the Supplementary Material with unit cell sizes equal to 1.5 and 2.5 mm. To simplify the calculations and following the mesh independence study performed in (Ruiz de Galarreta et al., 2020) the structures ($10 \times 10 \times 15$ unit cells) were meshed with quadratic Timoshenko beam elements (each of the struts was meshed with 6 elements) and a frictionless contact was defined between the structure and the rigid shells. The Gibson and Ashby curves were also derived for the FCC and OCT uniform structures.

2.3.2. Numerical modelling of porous graded structures with solid elements

The stiffness of the seven different porous graded structures with unit cell sizes equal to 1.5 mm (Fig. 2) was estimated by the FEA. Measurements of the actual manufactured struts, see 2.4.2, provided the input for the strut diameters used in the FE models. The FE specimen's width and the length was equal to the manufactured specimens, i.e. 10 unit cells; however for element reduction, the height of the structure was only set to 5 unit cells. The exception to this was for the longitudinally and longitudinally & radially graded structures, where the whole structure was modelled. The height independence study performed in (Ruiz de Galarreta et al., 2020) concluded that the height of the specimen only needed to be modelled with 5 units cells for a good approximation of the mechanical properties. In this work the influence of the number of cells in the height direction was also studied, by analysing three different structures (MRG, RG1 and LTG) with varying number of unit cells in height. The defined boundary conditions allowed normal displacement on symmetric faces to be constrained and thus only one quarter of the structure needed to be modelled. However, in the case of
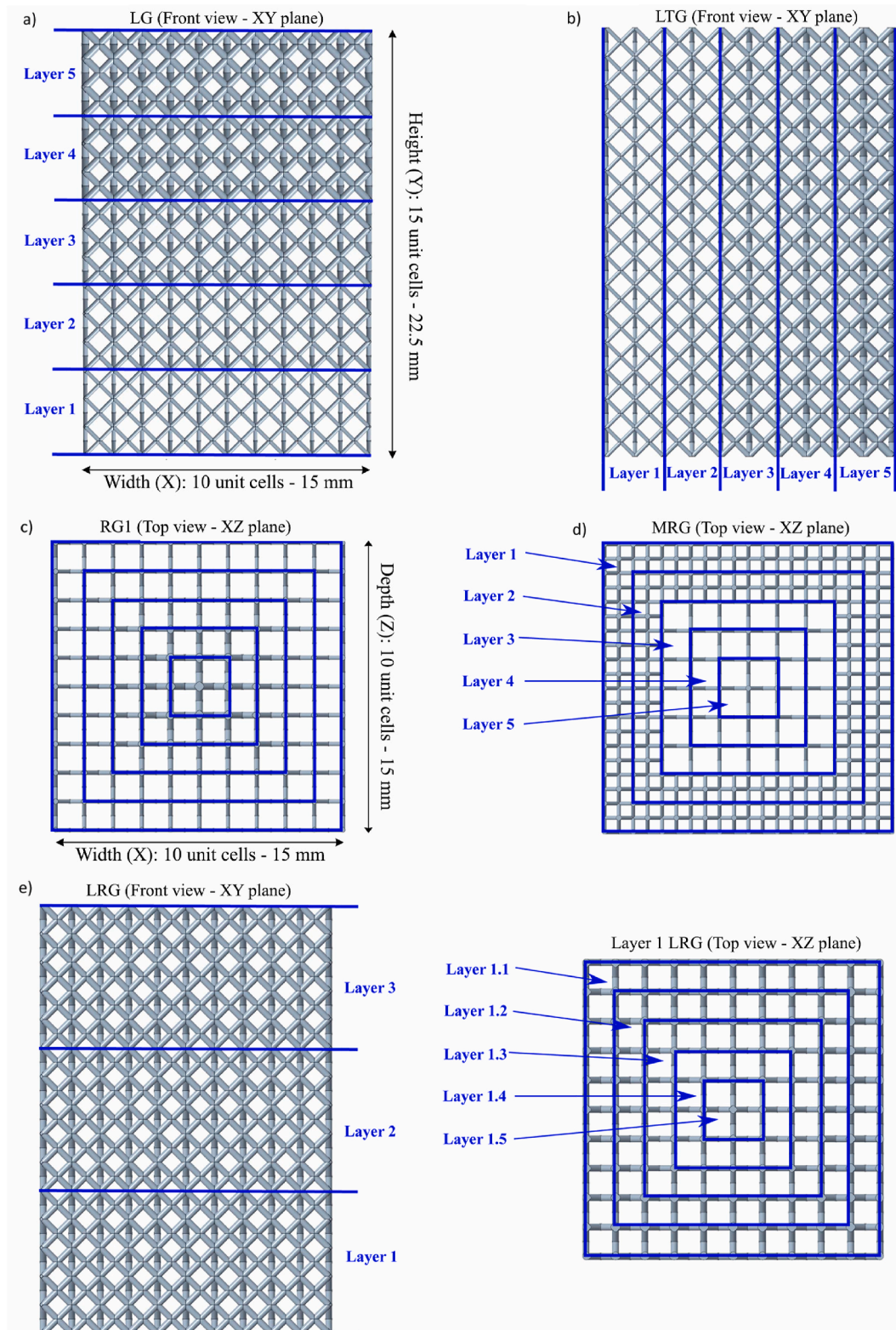
Fig. 2. Porous graded lattice structures a) LG structure, b) LTG structure, c) RG1 structure, d) MRG structure and e) LRG structure.

the lateral graded structures, half of the structure was studied. Symmetry boundary conditions were applied by constraining the displacement perpendicular to the plane of symmetry. The FEA boundary conditions utilised are seen in Fig. 3. To increase the accuracy of the FEA simulations all the models were meshed with 3D quadratic tetrahedral elements (C3D10) with an element size equal to 80 μm; and a friction

coefficient equal to 0.1 (Ruiz de Galarreta et al., 2020). Note, that the Gibson and Ashby curves for the FCC (Ruiz de Galarreta et al., 2020) and OCT lattice structures will be different with these new conditions.

Table 1
Bilinear elasto-plastic model of the SLM (Selective Laser Melting) stainless steel struts (Ruiz de Galarreta et al., 2020).

Young's Modulus [GPa]	Yield Stress [MPa]	Ultimate Strength [MPa]	Ultimate plastic strain [-]	Poisson's ratio [-]
81.3	263.3	575.3	0.22	0.3

2.3.3. Numerical modelling of porous graded structures with modified beam model

The beam model can significantly reduce the computational time, specially for big structures, however this FE model for lattice structures is only accurate for very low densities as stated in a previous work in the literature (Ruiz de Galarreta et al., 2020). While increasing the density of lattice structures, the difference in the elastic modulus between the solid and beam mesh increases exponentially. To account for this difference, in this work the stiffness matrix of each beam element has been artificially modified accordingly to its density by varying its base material elastic modulus (from E_0 to E_{new}). First, an exponential equation (Eq. (4)) determining the difference in the elastic modulus between tetrahedral and beam meshes has been fitted for the FCC and OCT structures. Then, for each unit cell type and relative density the new base material elastic modulus is derived with Eq. (5).

$$E_{diff} = K\left(\frac{\rho}{\rho_0}\right)^n \qquad (4)$$

$$E_{new} = E_0\left(1 + \frac{E_{diff}}{E_{beam}}\right) \qquad (5)$$

where E_0 and E_{new} represent the actual and new base material elastic modulus, E_{diff} the difference in elastic modulus between the solid and beam models and E_{beam} the equivalent elastic modulus of a uniform lattice structure derived from the beam model. The same procedure was followed with the yield strength.

The seven different porous graded structures were modelled with an in-house code in Matlab (in this case the whole geometry) and the corresponding new base material elastic modulus was set for each type of unit cell (FCC or OCT) and relative density. These values can be found in the supplementary material. Then the same procedure as stated in section 2.2.1 was followed. The results were compared to the ones derived with the solid model.

2.4. Experimental analysis

2.4.1. Sample design and manufacturing

For physical manufacture of the specimens, the functionally graded structures were designed in Rhino 6 as line-geometry. Structures were specified in a table of 7 columns and numerous rows, with every row specifying the co-ordinates of the two strut nodes as well as the diameter of the strut. Specimens had a 1.5 mm unit cell size. The cuboid test specimen size was 10 × 10 × 15 unit cells (15 × 15 × 22.5 mm) to meet the test specimen recommendations of Gibson & Ashby (Gibson and Ashby, 1997; Ashby et al., 2000) and the requirements of ISO 13314:2011. Software, developed in-house, generated the slice data (build files) as described in (Ghouse et al., 2017, 2018), with strut thickness being controlled by the laser parameters. Relationships between the manufactured diameter of the strut and the input laser parameters have been established previously (Ghouse et al., 2017).
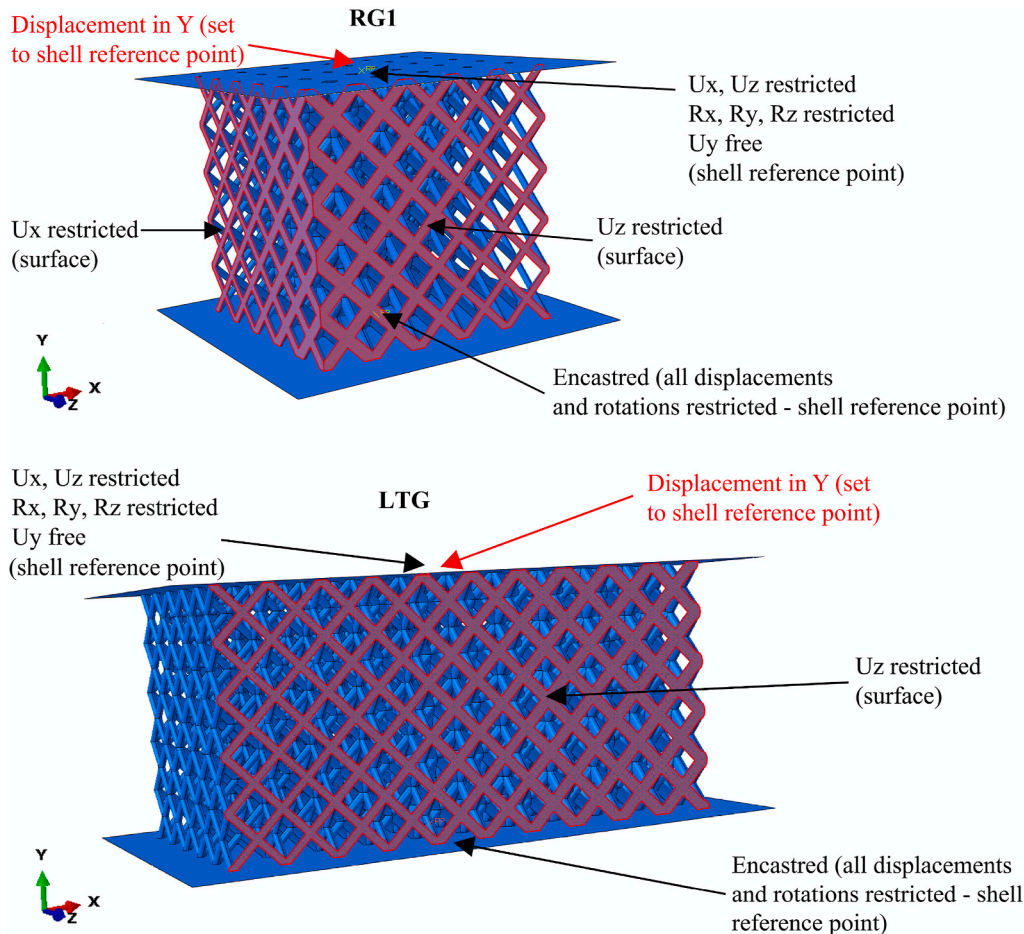

Fig. 3. FEA displacement and boundary conditions for the RG1 structure (top) and LTG structure (bottom).

Consequently, laser parameters were specified on a strut-by-strut, region-by-region or part-by-part basis to produce porous graded specimens. All specimens were manufactured on a Renishaw AM250 metal powder bed fusion system, described previously in detail (Ghouse et al., 2017, 2018) from Stainless Steel 316L powder (Carpenter Additive Ltd.). Electro discharge machining was used to cut the porous graded structures off the base plate. Specimens were ground parallel and cleaned in ethanol ultrasonically prior to testing and analysis.

2.5. Morphological analysis

The relative density of each graded structure was calculated by weighing the specimen dry in atmospheric conditions and dividing the measured mass by the solid macro volume mass, assuming a density of 8.1 g/cm^3, this was repeated on 5 identical samples per unique structure. The macro dimensions of the structure were measured by Vernier callipers. Scanning electron microscopy (Hitachi S–3400N) was utilised to image each structure. The diameter or thickness of the strut was measured on the resulting images via ImageJ in 20 locations and averaged.

2.5.1. Quasi static compression testing

A material testing machine (Instron 8872) equipped with a 10 kN load-cell was utilised to compressively test the lattices to ISO 13314:2011. A constant compression/rate of 2 mm/min was maintained for all specimens. For each unique porous graded structure, to estimate the plateau strength, an initial sample was compressed to 50% strain and the average stress between 20 and 30% strain was calculated. These initial samples were also used to analyse the failure mode of each structure. Following this, samples of the same structure type (n = 3) were compression tested with a hysteresis loop between 70% and 20% of the estimated plateau strength, tests were ended at 50% strain. The purpose of the hysteresis loop is to account for localized plasticity in porous structures which decreases the initial loading curve's slope (Ashby et al., 2000). Two LVDTs (RDP D6/05000A) recording at 30Hz were used to measure displacement between the platens. The average recorded displacement divided by the initial height of the specimen was defined as strain. Stress (σ) was calculated by dividing the measured load from the load-cell by the initial cross-sectional area of the specimen (i.e. the initial width & length). Elastic modulus *(E)* was calculated via linear regression of the hysteresis loop and yield strength (σ_y) was the intersection of the stress-strain curve and a 1.0%, relative to the elastic modulus, plastic compressive strain offset curve.

3. Results

3.1. Analytical models vs FEA

The Gibson and Ashby curves for the elastic modulus of the uniform FCC and OCT lattice structures are represented in Fig. 4. One curve (solid line) is derived from FEA by modelling the structures with beam elements and a frictionless contact, while the other curve (dash line) is derived from FEA by meshing the structures with tetrahedral elements and defining a friction contact equal to 0.1. The difference between the models is greater for high relative densities, as the ratio of strut length: diameter is smaller and therefore at high relative densities the beam model is not a good approximation. There is also a difference between the two models due to the difference in the contact properties.

The stiffness values estimated by the analytical models and FEA of the different structures analysed in this section can be found in the supplementary material. The accuracy of the analytical models has an average mean error (S.D.) of 7.7% (9.4%). The minimum difference between the analytical models and the FEA is seen with the hybrid radial porous graded structures with an average error equal to 0.13% (0.08%), while the maximum error between the approaches is seen with the longitudinal graded structures 14.5% (14.8%).

3.2. Experimental results

The measured strut thickness for each of the structure regions is displayed in Table 2. These strut diameter values were used in the FEA models.

The failure mode of the RG, MRG, LTG and MLTG structures is similar, showing a homogenous ductile failure as shown in Fig. 5 (MLTG stress-strain curve is very similar to MRG stress-strain curve and it is not shown in the figure). In the case of the LG and LRG structures, the failure mode is represented by the collapse (crushing) of layer by layer (Fig. 5). In the LG structure it can be observed clearly that there are 5 steps, each representing the collapse of each layer. The sequential layer collapse can be seen in the step-like features of the stress-strain curves.

3.3. FEA results

3.3.1. FEA with solid elements

The effect of how many unit cells are modelled in the height versus the modulus of the graded structures was analysed for the MRG, RG1 and LTG structures and is displayed in Fig. 6. The difference in modulus between modelling 5 versus 6 unit cells in height is lower than 3% and therefore to reduce computational cost, 5 unit cells were modelled in height for all structures, except for the LG and LRG structures.

The relative density of the FGPS (excluding the hybrid structures) is displayed in Table 3. The displayed relative density is obtained from the
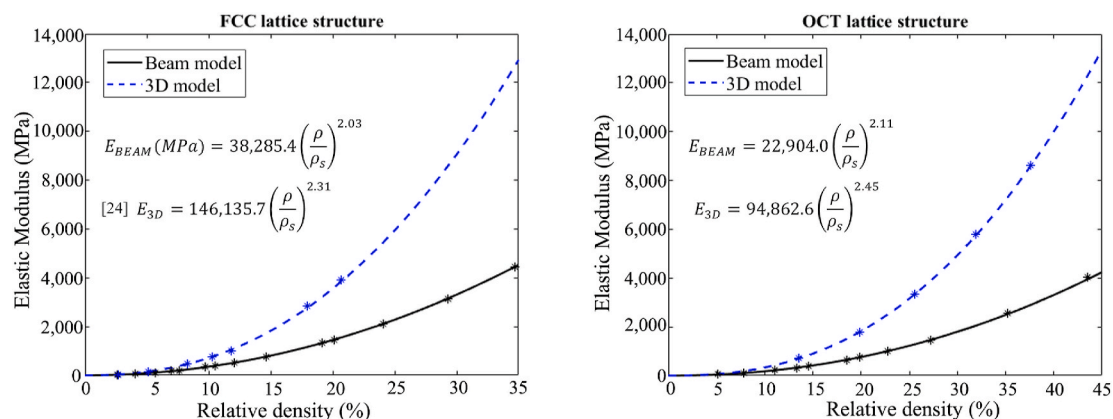

Fig. 4. Gibson and Ashby curves for the FCC and OCT unit cells.

$$E_{BEAM}(MPa) = 38,285.4\left(\frac{\rho}{\rho_s}\right)^{2.03}$$

$$[24]\ E_{3D} = 146,135.7\left(\frac{\rho}{\rho_s}\right)^{2.31}$$

$$E_{BEAM} = 22,904.0\left(\frac{\rho}{\rho_s}\right)^{2.11}$$

$$E_{3D} = 94,862.6\left(\frac{\rho}{\rho_s}\right)^{2.45}$$

Table 2
Strut diameters mean (S.D.) measured from the lattice structures (in μm).

	LG	RG1	RG2	LTG	MRG	MLTG
Layer 1	207.8 (7.8)	206.8 (26.3)	373.3 (15.1)	206.8 (26.3)	206.2 (10.3)	206.2 (10.3) FCC & OCT
Layer 2	249.1 (9.9)	241.3 (6.7)	344.9 (10.2)	241.3 (6.7)	FCC & OCT	
Layer 3	306.8 (14.3)	289.3 (11.3)	289.3 (11.3)	289.3 (11.3)		
Layer 4	372.9 (19.3)	344.9 (10.2)	241.3 (6.7)	344.9 (10.2)		
Layer 5	395.4 (9.1)	373.3 (15.1)	206.8 (26.3)	373.3 (15.1)		

LRG

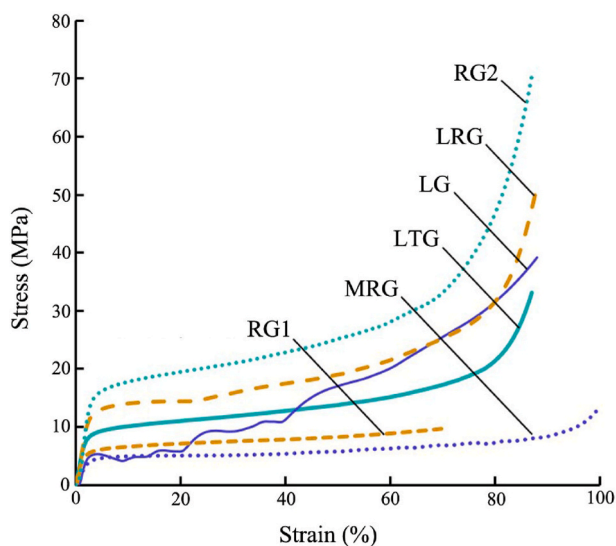|	Radial Layer 1	Radial Layer 2	Radial Layer 3	Radial Layer 4	Radial Layer 5
Layer 1	344.9 (10.2)	289.3 (11.3)	241.3 (6.7)	206.8 (26.3)	206.8 (26.3)
Layer 2	344.9 (10.2)	289.3 (11.3)	289.3 (11.3)	241.3 (6.7)	241.3 (6.7)
Layer 3	344.9 (10.2)	344.9 (10.2)	289.3 (11.3)	289.3 (11.3)	289.3 (11.3)

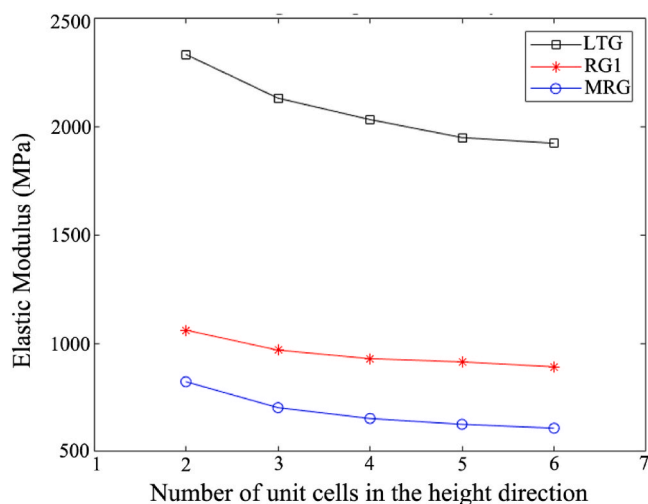**Fig. 5.** Experimental stress-strain curves of the FGPSs.

Fig. 6. Height independence study of the FGPS.

Table 3
FEA relative density, elastic modulus and yield strength of the FGPS and elastic modulus and yield strength of uniform lattice structures with the corresponding relative density.

	LG	RG1	RG2	LTG	LRG
(ρ/ρ_s)	0.157	0.106	0.178	0.142	0.157
E_{graded} [MPa]	1065.2	913.9	3137.1	1947.8	2046.9
$E_{uniform}$ [MPa]	2029.0	818.9	2711.6	1609.0	2029.0
$\sigma_{y,graded}$ [MPa]	5.17	6.18	17.97	11.77	12.06
$\sigma_{y,uniform}$ [MPa]	12.82	6.19	16.17	10.64	12.82

ideal structures designed with the corresponding strut diameters (Table 2). Yield strength and elastic modulus results obtained by FEA are also displayed together with values of uniform porous structures with the corresponding relative density. The latter values were obtained from previously obtained Gibson and Ashby curves (Ruiz de Galarreta et al., 2020).

The structures where the porosity gradient is parallel to the loading direction (LG structure) have a lower elastic modulus and lower yield strength than uniform porous lattice structures with the same relative density. This difference in the modulus and yield stress is understandable as the LG will collapse first in the bottom layer, where the relative density is lower than uniform porous structures. As can be seen in Fig. 7, the bottom layer, composed of thinner struts, has the greatest von mises stresses and is therefore the first to collapse. It can be observed that the stress concentration appears close to the node regions forming a plastic hinge. In contrast, for the structures where the porosity gradient is perpendicular to the direction of loading (RG1, RG2 and LT structures) the von mises stress is distributed more homogeneously between layers as can be seen in Fig. 7.

This can also be observed when analysing the deformation in structures where the porosity gradient is parallel or perpendicular to the direction of loading. Fig. 8 illustrates the relative strain of each layer with respect to the lattice structure strain for LG and RG2 structures. The maximum von mises stress for each layer is also shown in the figure. As it can be observed, from the beginning of the LG structure deformation, the weakest layer (layer 1) takes most of the LG structure strain (around 55%). At 0.4% of strain, the plastic hinge is formed in layer 1 thus the relative strain of this layer with respect to the total strain increases. Looking at the von mises stress, it can be observed that only layer 1 and 2 has reached the yield strength of the material (263.3 MPa – Table 1). In contrast, when analysing the RG2 structure, it can be observed that all the layers have the same strain and the difference in maximum von mises stress between layers is not so high. As one can expect, if all the layers have the same strain, the layers with higher relative density (higher stiffness) will carry higher loads than the rest of the layers.

In the RG1, RG2 and LT structures the elastic modulus is 11.6%, 15.7% and 21.1% greater than their corresponding uniform porous structures. The yield strength is 11.1% and 10.6% greater for RG2 and LTG structures, and 0.2% lower for RG1 structure. For the LRG structure where the porosity gradient is in both directions, perpendicular and parallel to the loading direction, differences with the uniform porous structure will depend on the relative density of the weaker layer in the longitudinal direction. Table 4 displays the stiffness & strength to weight ratios for all the porous graded structures and their corresponding uniform porous structures. From the structures analysed in this work, the RG2 structure has the highest strength-weight and stiffness-weight ratio, while the hybrid structures have the lowest values. This is understandable as the second unit cell type used in these structures (OCT unit cell) is less stiff than the FCC unit cell as can be seen in Fig. 4. If the hybrid structures are not considered, the LG structure has the lowest stiffness & strength - weight ratios which is expected, as both the stiffness and strength of the structure are mostly defined by the weakest layer of the structure. It can also be observed that the structures where there is no change in strut diameter (MRG and MLTG) have the highest strength-
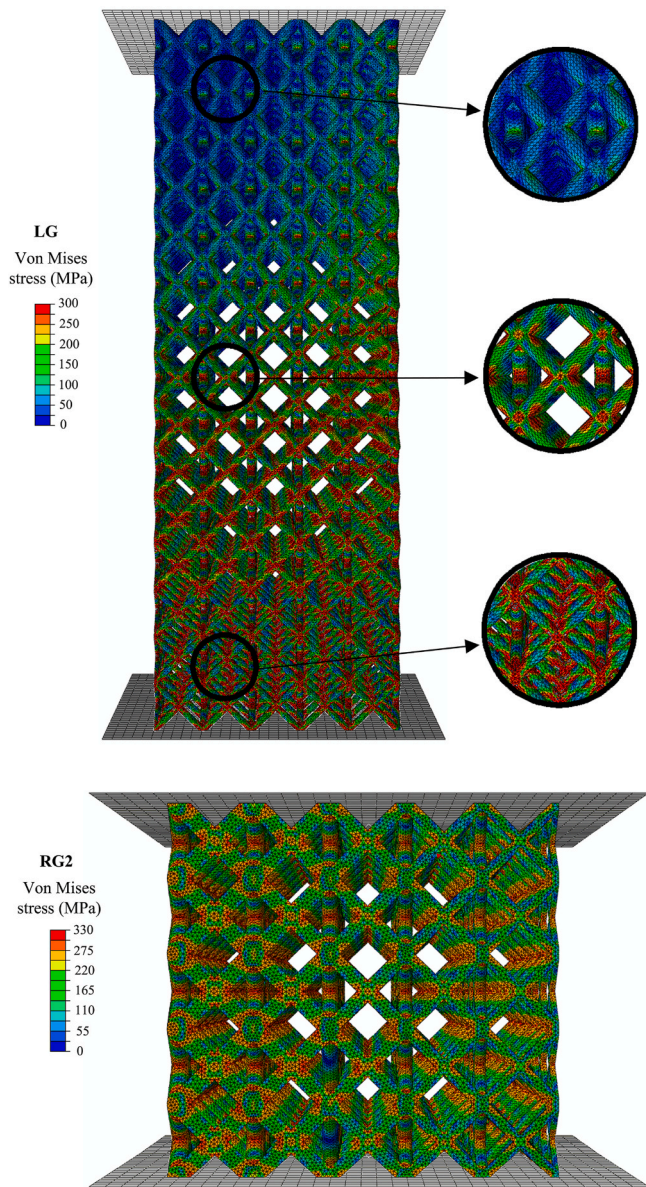
Fig. 7. FEA Von Mises stress distribution of the a) LG and b) RG2 structures.

stiffness ratio.

3.3.2. FEA with beam elements

The difference in the equivalent elastic modulus of uniform lattice

structures between the tetrahedral and beam mesh for the FCC and OCT structures is illustrated in Fig. 9. The new base material data for each of the layers is displayed in the Supplementary Material.

The results of the simulations indicate an acceptable accuracy for the beam models, with an average difference (SD) in the equivalent elastic modulus and yield strength between the solid and beam model equal to 4.6% (3.7%) and 6.1% (5.7%), respectively. The maximum difference was found in the LG structure, 11.8% in the elastic modulus and 17.6% in the yield strength. The comparison between the solid and beam models for the seven FGPSs is displayed in Table 5. In order to show the computational time reduction, the number of degrees of freedom is also displayed in the table. It should be noted that for the beam model the whole structure was modelled and symmetry was not applied.

3.4. Numerical and experimental results

The experimental, solid FE model and analytical elastic modulus of the fabricated structures are illustrated in Fig. 10 and displayed in Table 6. It should be noted that the unit cell size of all these structures is 1.5 mm. In the case of the longitudinal graded structures (LG and LRG), the elastic modulus was derived from the first slope of the stress-strain curves. The mean error (SD) between the FEA with solid elements and the experiments is 8.7% (7.0%). The lowest errors are found in the hybrid lattice structures composed of the FCC and OCT unit cells where the strut diameter is constant. In the case of the LG and LRG structure, despite having the same relative density, the LRG structure is significantly stiffer due to the orientation of the structure.

The results from the FEA and the analytical models are very close, with an average difference equal to 3.5% (2.4%). As in section 3.1, the analytical model is closer to the FEA results for the hybrid structures where there is no change in the strut diameter.

Numerical and experimental yield strength values are illustrated in Fig. 11. The mean difference (SD) between the yield strength between the FEA and experimental data is greater than the elastic modulus, 15.01% (10.48%, Table 7). Similarly, the difference between the FEA

Table 4
Stiffness-weight, strength-weight and strength-stiffness ratio of the analysed porous graded structures. In parenthesis the ratios of their corresponding uniform porous structures.

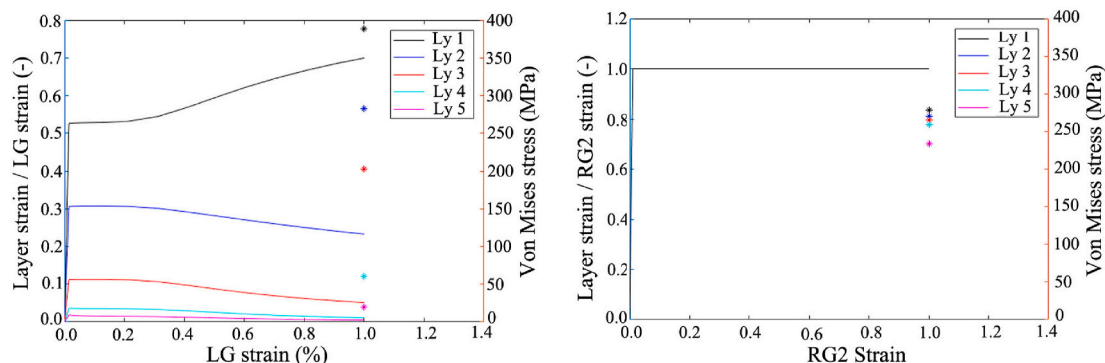|	Stiffness-weight ratio [MPa/g]	Strength-weight ratio [MPa/g]	Strength-stiffness ratio (x10³) [-]
LG	165.5 (315.2)	0.80 (1.99)	4.83 (6.31)
RG1	210.3 (188.4)	1.42 (1.42)	6.75 (7.54)
RG2	429.8 (371.5)	2.46 (2.22)	5.72 (5.98)
LTG	334.5 (276.3)	2.02 (1.83)	6.04 (6.62)
LRG	317.9 (315.2)	1.87 (1.99)	5.88 (6.31)
MRG	130.6	1.13	8.65
MLTG	127.1	1.10	9.08

Fig. 8. Relative layer strain for LG (left) and RG2 (right) structures. Maximum von mises points for each layer represented with dots.
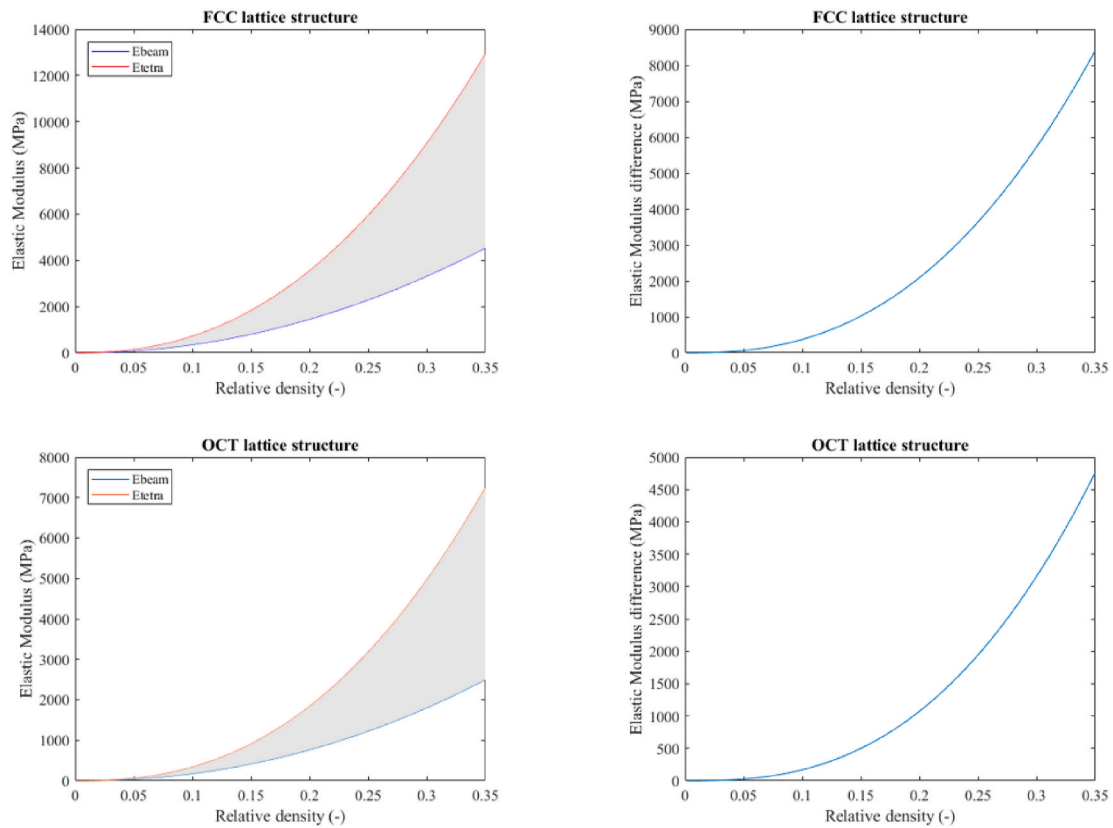
Fig. 9. Difference in the equivalent elastic modulus for the FCC (top) and OCT (bottom) structures. Beam and solid model (left) and difference (right).

Table 5
Degrees of freedom, elastic modulus and yield strength of the porous graded structures for the solid and beam FE models.

|	d.o.f. ($*10^5$)		Elastic modulus [MPa]			Yield strength [MPa]		
	Solid model	Beam model	Solid model	Beam model	Differ. (%)	Solid model	Beam model	Differ. (%)
LG	174.4	7.4	1065.2	1190.6	11.8	5.17	6.08	17.6
RG1	49.2	7.4	913.9	923.29	1.0	6.18	6.44	4.2
RG2	69.4	7.4	3137.1	3026.3	3.5	17.97	17.93	0.2
LTG	115.0	7.4	1947.8	1848.5	5.1	11.77	11.49	2.4
LRG	198.1	7.4	2046.9	2183.0	6.6	12.06	13.09	8.5
MRG	57.9	16.7	626.4	635.6	1.5	5.40	5.64	4.5
MLTG	106.0	15.3	557.5	571.7	2.6	4.83	5.09	5.5
			Average (S.D)		4.6 (3.7)	Average (S.D)		6.1 (5.7)
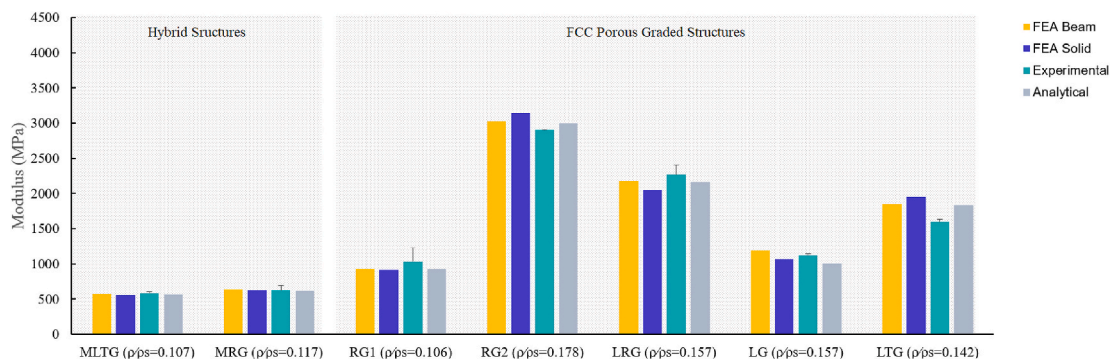
Fig. 10. Experimental, FEA and analytical elastic modulus of the FGPSs.

and analytical results are greater for the yield strength 10.69% (18.40%). Again, the analytical model is more accurate for the hybrid structures.

4. Discussion

Functionally graded porous structures are unique materials

Table 6
Experimental, FEA and analytical elastic modulus of the porous graded structures.

	Experimental [MPa]	FEA [MPa]	Analytical [MPa]	Difference Exp. Vs FEA	Difference FEA vs Anal. (%)
LG	1120	1065.2	1009.2	4.9	5.3
RG1	1033	913.9	925.4	11.5	1.3
RG2	2898	3137.1	3000.2	8.3	4.4
LTG	1596	1947.8	1832.9	22.0	5.9
LRG	2265	2046.9	2114.4	9.6	3.3
MRG	625	626.38	618.8	0.2	1.2
MLTG	584	557.46	560.5	4.5	0.5
		Average (S.D)		8.7 (7.0)	3.5 (2.4)

possessing variations in their structure all through their volume to produce tailored properties. This allows for greater optimisation both locally and globally in a component of mechanical properties such as enhanced strength:weight, stiffness:weight, strength:stiffness and energy absorption as well as thermal and acoustic properties. Particularly in joint replacements where the density and stiffness of bone varies both locally at joints and throughout the skeleton, the integration of FGPS into orthopaedic implants represents an exciting new development to biomechanically match implants to the native tissue.

In this work the behaviour of seven different porous graded structures have been analysed analytically, experimentally and numerically. Two different FEA procedures have been studied: 1) an existing FEA methodology for uniform porous structures using solid elements and 2) a novel FEA methodology using beam elements with a modified stiffness matrix. Both approaches have been found to accurately predict the elastic properties of any FGPS independently of the porosity grading direction. While the average error in the elastic modulus of the FGPS is less than 10% for the first methodology, the average difference between the beam model and solid model was found to be less than 5%. It should be noted that while the simulations for the solid models can take from 1 to 3 days, the simulations for the beam models can be run in less than 20 min. Although the first methodology would represent local stresses in the struts more accurately, the second approach drastically reduces the computational time making it ideal when designing and analysing components composed of big FGPS where modelling them with solid elements is prohibitive. This finding provides two methods of rapidly designing porous graded structures to meet structural requirements before they are manufactured. The FEA results can also help when analysing the fatigue performance of these structures, which is still relatively undefined (Maconachie et al., 2019). For instance, local tensile stresses can help in developing an analytical fatigue life model for these structures (Lietaert et al., 2018).

It was experimentally observed that the deformation behaviour of FGPSs depends on the porosity gradient direction. Failure mode of structures with porosity gradient perpendicular to the load direction (RG, MRG, LTG and MLTG) show a homogenous ductile failure. The

deformation is similar to uniform porous structures and three main stages can be observed: a linear elastic deformation, a plateau region and finally a densification region. These results are in accordance with other results in the literature where radially (Zhang et al., 2019) and laterally (Yang et al., 2019) graded porous structures are studied. In contrast, for the structures, where the porosity gradient direction is parallel to the load direction (LG), the failure mode is represented by the collapse of each layer. These results are also in accordance with other results in the literature (Maskery et al., 2016; Zhao et al., 2020; Al-Saedi et al., 2018). This deformation behaviour was also observed in the LRG structure, where the porosity is graded in both directions.

The results also show that radially graded porous structures outperform the behaviour of their corresponding uniform porous structure under compression loads in stiffness:weight (11.6% and 15.7% increase of the elastic modulus for the RG1 and RG2 structures), which is expected, as the rule of mixtures for composite materials (Eq. (2)) is a linear equation while Gibson and Ashby equation (Eq. (3)) is exponential. A simple case is represented in Fig. 12. A radially graded porous structure which has a relative density of 0.1 in the outer layer (50% of the total volume) and a relative density of 0.3 in the inner layer (50% of the total volume). The corresponding uniform porous structure would have a relative density equal to 0.2. As can be seen in Fig. 12, the elastic modulus under compression will be higher for the radially graded porous structure represented by the linear equation of the rule of mixtures. In contrast, the elastic modulus of longitudinally graded porous structures will be highly influenced by the collapse of the weakest layer of the porous graded structure, and therefore weaker than a uniform porous structure of similar relative density.

Analysis on the mechanical behaviour of graded porous structures is mostly limited to experiments. There are few studies comparing the numerically and experimentally derived mechanical properties of metal graded porous structures. Zhao et al. (2020) analysed two types of unit cells, the primitive and gyroid TPMS, grading the porosity in the axial direction. The difference found in the elastic modulus was 26.5% and 38.9%, respectively. The same type of porous graded structure was analysed by Zhou et al. (2020) comparing the network and sheet based

Table 7
Experimental, FEA and analytical yield strength of the porous graded structures.

	Experimental [MPa]	FEA [MPa]	Analytical [MPa]	Difference Exp. Vs FEA	Difference FEA vs Anal. (%)
LG	4.69	5.17	7.86	10.23	52.03
RG1	5.99	6.18	6.45	3.17	4.37
RG2	15.43	17.97	17.25	16.46	4.01
LTG	8.92	11.77	11.25	31.95	4.40
LRG	12.01	12.06	13.05	0.42	8.21
MRG	4.33	5.40	5.32	24.71	1.37
MLTG	4.09	4.83	4.85	18.09	0.42
		Average (S.D)		15.01 (10.48)	10.69 (18.40)
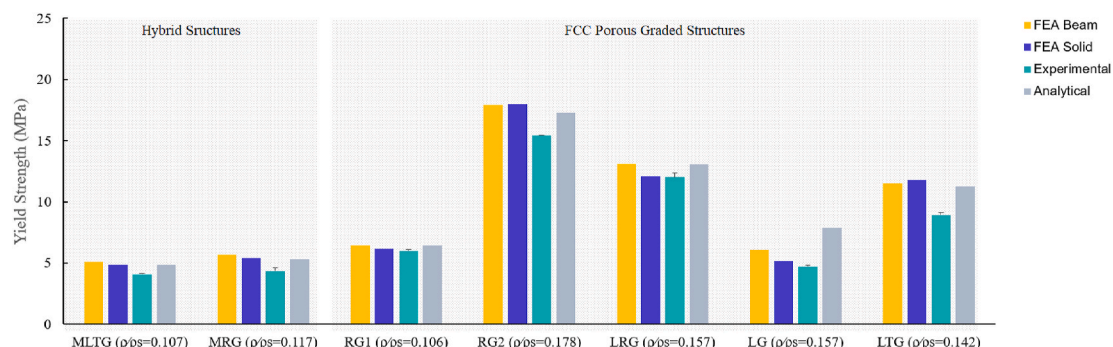
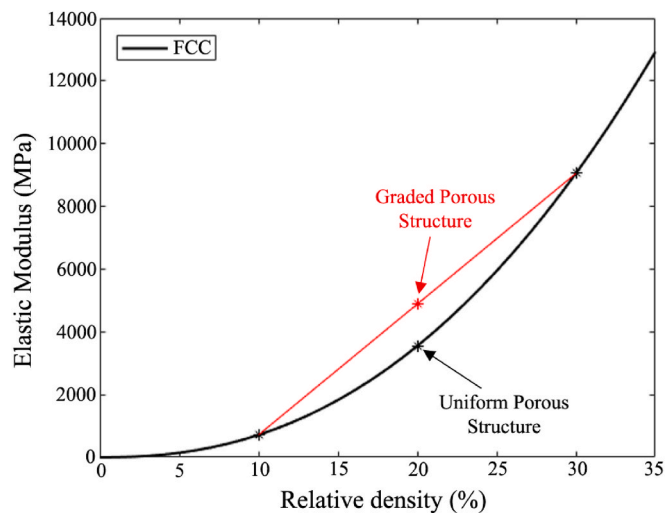**Fig. 11.** Experimental, FEA and analytical yield strength of the FGPSs.

Fig. 12. Radially porous graded structure vs Uniform porous structure.

Gyroid TPMS. The average error found in the elastic modulus and yield strength was 29.9% and 28.3% respectively. Al-Saedi et al. (2018) analysed the energy absorption of a F2BCC axially graded structure, but the elastic modulus of the graded structure was much higher for the experimental test than from the numerical study. Zhang et al. (2019) analysed one radially graded porous structure formed by a diamond unit cell. The error between experiments and FEA for the elastic modulus was only 4.6% (18.8% for the ideal model). While accurate, this method relies on micro-CT scanning to measure strut diameter deviations and defects. With respect to the analytical models, as previously reported, both the Kelvin-Voight model and the rule of mixtures are good tools to estimate the elastic modulus of the structures versus FEA (Yang et al., 2019; Maskery et al., 2018; Zhang et al., 2019). Maskery et al. (2018). found an error between the Kelvin-Voight model and FEA results ranging from 10% to 14% when analysing longitudinally porous graded TPMS structures (Maskery et al., 2018). Zhang et al. analysed radially graded porous structures finding an error between the FEA and the rule of mixtures around 4% (Zhang et al., 2019). The average error found in this work is similar for the fabricated structures (3.5%). The average error found in the structures which have been modelled with beam elements is also low, 7.7%. From this analysis it can be concluded that the analytical models more accurately predict the elastic modulus of radially graded porous structures than longitudinally graded porous structures.

Some differences in the elastic modulus between experimental and FEA results were noticed in this study. These might be attributed to small errors in the strut diameter measurements. Differences in the yield strength between experiments and FEA (around 16%), may be due to other source of errors: the elasto-plastic material model overpredicting the FEA yield strength by around 4% (Ruiz de Galarreta et al., 2020), structural irregularities such as strut waviness and residual stresses which is likely present in the structures, and these factors are not accounted in the FEA model. A possible source of the error between FEA and analytical models is the stress concentrations in the node regions due to the change in strut diameters. For instance, L7 and L10 have a longitudinally porosity gradient with strut diameter ranging from 0.2 mm to 0.4 mm (Table S1). While in L10 there are only 3 different layers, the L7 structure has 5 different layers, making the strut diameter transition more smoothly. This smooth transition contributes to the low error of the L7 structure (4.5%) compared to L10 (25.9%). In the case of the hybrid structures, where there is no change in strut diameter, the analytical models predict the elastic modulus of the structures very accurately with average difference equal to 0.1%.

A drawback of this work is that the elastic properties of the structures were derived only for one direction, while the structures presented in

this work are transversely isotropic. In an ongoing work, we are analysing other elastic properties (young's and shear modulus, Poisson's coefficients) required to completely define the stiffness matrix of the structure. It should be also mentioned, that a single Young's modulus derived from our previous work (Ruiz de Galarreta et al., 2020) was used to define the isotropic material model for all the structures. Recently it was also observed that building angle direction and strut diameter do not affect the Young's modulus and neither the yield strength for SS316L (Hossain et al., 2021). Another disadvantage of the procedures analysed in this work is that they are only valid to study the elastic properties of the structures (the first region of the stress-strain curves) and they are not valid for instance to define the energy absorption of the structures. However, for many applications the FGPSs will work in the elastic region.

5. Conclusion

The mechanical behaviour of seven different Stainless Steel 316L porous graded structures manufactured by laser powder bed fusion was experimentally and numerically investigated. The porosity gradient in the structures was achieved by either: 1) varying the strut diameter or 2) combining two types of unit cells (FCC and OCT). The porosity gradient was designed in different directions: longitudinally, laterally, radially and longitudinally & radially. The following conclusions are derived from the study:

1) A FEA procedure described in the literature for uniform porous graded structures is appropriate to analyse different porous graded structures. The yield strength and elastic modulus values of the porous graded structures are predicted by FEA with good accuracy.
2) A novel FEA procedure, which drastically reduces the computational time, is proposed to model with accuracy different functionally graded porous structures.
3) The FEA results show that the stress concentration appear close to the node regions and depend on the porosity gradient direction. For longitudinally structures it can be observed that when the plastic hinge is formed in the weakest layer, the relative strain of that layer increases. In contrast, for structures with porosity gradients perpendicular to the direction of loading, the von mises stress is more homogeneously distributed between layers.
4) The Kelvin-Voight model and rule of mixtures are also an accurate tool to predict the yield strength and elastic modulus of porous graded structures, especially for structures with a smooth transition of the strut diameter. The accuracy for hybrid structures, where there is no change in the strut diameter was found to be very high.
5) The experimental and numerical analysis show that porous structures with graded porosity in the perpendicular direction to the load have higher yield strength and elastic modulus than the corresponding uniform structures. In the case of the structures with a porosity gradient parallel to the load direction, these values will primarily depend on the weakest layers of the structure.

CRediT authorship contribution statement

Sergio Ruiz de Galarreta: Conceptualization, Methodology, Formal analysis, Investigation, Writing – original draft. **Ruben J. Doyle:** Formal analysis, Visualization, Writing – review & editing. **Jonathan Jeffers:** Writing – review & editing, Supervision, Funding acquisition. **Shaaz Ghouse:** Conceptualization, Validation, Investigation, Writing – review & editing.

Declaration of competing interest

The authors declare that they have no known competing financial interests or personal relationships that could have appeared to influence the work reported in this paper.

Acknowledgements

Appendix A. Supplementary data

Supplementary data related to this article can be found at https://doi.org/10.1016/j.jmbbm.2021.104784.

Data availability

The raw data required to reproduce these findings are available to download from rdm-enquiries@imperial.ac.uk. The processed data required to reproduce these findings are available to download from rdm-enquiries@imperial.ac.uk.

References

Al-Ketan, O., Lee, D.W., Rowshan, R., Abu Al-Rub, R.K., 2020. Functionally graded and multi-morphology sheet TPMS lattices: design, manufacturing, and mechanical properties. J. Mech. Behav. Biomed. Mater. 102, 103520. https://doi.org/10.1016/j.jmbbm.2019.103520.

Al-Saedi, D.S.J., Masood, S.H., Faizan-Ur-Rab, M., Alomarah, A., Ponnusamy, P., 2018. Mechanical properties and energy absorption capability of functionally graded F2BCC lattice fabricated by SLM. Mater. Des. 144, 32–44. https://doi.org/10.1016/j.matdes.2018.01.059.

Ashby, M.F., 2006. The properties of foams and lattices. Philos. Trans. R. Soc. A Math. Phys. Eng. Sci. 364, 15–30. https://doi.org/10.1098/rsta.2005.1678.

Ashby, M., Evans, T., Fleck, N., Hutchinson, J., Wadley, H., Gibson, L., 2000. Metal Foams A Design Guide. Elsevier.

Bai, L., Gong, C., Chen, X., Sun, Y., Xin, L., Pu, H., Peng, Y., Luo, J., 2020. Mechanical properties and energy absorption capabilities of functionally graded lattice structures: experiments and simulations. Int. J. Mech. Sci. 182, 105735. https://doi.org/10.1016/j.ijmecsci.2020.105735.

Blázquez-Carmona, P., Sanz-Herrera, J.A., Martínez-Vázquez, F.J., Domínguez, J., Reina-Romo, E., 2021. Structural optimization of 3D-printed patient-specific ceramic scaffolds for in vivo bone regeneration in load-bearing defects. J. Mech. Behav. Biomed. Mater. 121 https://doi.org/10.1016/j.jmbbm.2021.104613.

Ghouse, S., Babu, S., Van Arkel, R.J., Nai, K., Hooper, P.A., Jeffers, J.R.T., 2017. The influence of laser parameters and scanning strategies on the mechanical properties of a stochastic porous material. Mater. Des. 131, 498–508. https://doi.org/10.1016/j.matdes.2017.06.041.

Ghouse, S., Babu, S., Nai, K., Hooper, P.A., Jeffers, J.R.T., 2018. The influence of laser parameters, scanning strategies and material on the fatigue strength of a stochastic porous structure. Addit. Manuf. 22, 290–301. https://doi.org/10.1016/j.addma.2018.05.024.

Ghouse, S., Reznikov, N., Boughton, O.R., Babu, S., Ng, K.C.G., Blunn, G., Cobb, J.P., Stevens, M.M., Jeffers, J.R.T., 2019. The design and in vivo testing of a locally stiffness-matched porous scaffold. Appl. Mater. Today. 15, 377–388. https://doi.org/10.1016/j.apmt.2019.02.017.

Gibson, L.J., Ashby, M.F., 1997. Cellular Solids. Cambridge University Press, Cambridge. https://doi.org/10.1017/CBO9781139878326.

Han, C., Li, Y., Wang, Q., Wen, S., Wei, Q., Yan, C., Hao, L., Liu, J., Shi, Y., 2018. Continuous functionally graded porous titanium scaffolds manufactured by selective laser melting for bone implants. J. Mech. Behav. Biomed. Mater. 80, 119–127. https://doi.org/10.1016/j.jmbbm.2018.01.013.

Hedayati, R., Sadighi, M., Mohammadi-Aghdam, M., Zadpoor, A.A., 2016. Mechanics of additively manufactured porous biomaterials based on the rhombicuboctahedron unit cell. J. Mech. Behav. Biomed. Mater. 53, 272–294. https://doi.org/10.1016/j.jmbbm.2015.07.013.

Herrera, A., Yánez, A., Martel, O., Afonso, H., Monopoli, D., 2014. Computational study and experimental validation of porous structures fabricated by electron beam melting: a challenge to avoid stress shielding. Mater. Sci. Eng. C 45, 89–93. https://doi.org/10.1016/j.msec.2014.08.050.

Hossain, U., Ghouse, S., Nai, K., Jeffers, J.R.T., 2021. Mechanical and morphological properties of additively manufactured SS316L and Ti6Al4V micro-struts as a function of build angle. Addit. Manuf. 46, 102050. https://doi.org/10.1016/j.addma.2021.102050.

Jetté, B., Brailovski, V., Dumas, M., Simoneau, C., Terriault, P., 2018. Femoral stem incorporating a diamond cubic lattice structure: design, manufacture and testing. J. Mech. Behav. Biomed. Mater. 77, 58–72. https://doi.org/10.1016/j.jmbbm.2017.08.034.

Lietaert, K., Cutolo, A., Boey, D., Van Hooreweder, B., 2018. Fatigue life of additively manufactured Ti6Al4V scaffolds under tension-tension, tension-compression and compression-compression fatigue load. Sci. Rep. 8, 1–9. https://doi.org/10.1038/s41598-018-23414-2.

Limmahakhun, S., Oloyede, A., Sitthiseripratip, K., Xiao, Y., Yan, C., 2017a. Stiffness and strength tailoring of cobalt chromium graded cellular structures for stress-shielding reduction. Mater. Des. 114, 633–641. https://doi.org/10.1016/j.matdes.2016.11.090.

Limmahakhun, S., Oloyede, A., Chantarapanich, N., 2017b. Alternative designs of load – sharing cobalt chromium graded femoral stems. Mater. Today Commun. 12, 1–10. https://doi.org/10.1016/j.mtcomm.2017.05.002.

Liu, F., Mao, Z., Zhang, P., Zhang, D.Z., Jiang, J., Ma, Z., 2018a. Functionally graded porous scaffolds in multiple patterns : new design method , physical and mechanical properties. Mater. Des. 160, 849–860. https://doi.org/10.1016/j.matdes.2018.09.053.

Liu, F., Mao, Z., Zhang, P., Zhang, D.Z., Jiang, J., Ma, Z., 2018b. Functionally graded porous scaffolds in multiple patterns : new design method , physical and mechanical properties. Mater. Des. 160, 849–860. https://doi.org/10.1016/j.matdes.2018.09.053.

Maconachie, T., Leary, M., Lozanovski, B., Zhang, X., Qian, M., Faruque, O., Brandt, M., 2019. SLM lattice structures: properties, performance, applications and challenges. Mater. Des. 183, 108137. https://doi.org/10.1016/j.matdes.2019.108137.

Mahbod, M., Asgari, M., 2019. Elastic and plastic characterization of a new developed additively manufactured functionally graded porous lattice structure: analytical and numerical models. Int. J. Mech. Sci. 155, 248–266. https://doi.org/10.1016/j.ijmecsci.2019.02.041.

Maskery, I., Aboulkhair, N.T., Aremu, A.O., Tuck, C.J., Ashcroft, I.A., Wildman, R.D., Hague, R.J.M., 2016. Materials Science & Engineering A A mechanical property evaluation of graded density Al-Si10-Mg lattice structures manufactured by selective laser melting. Mater. Sci. Eng. 670, 264–274. https://doi.org/10.1016/j.msea.2016.06.013.

Maskery, I., Aremu, A.O., Parry, L., Wildman, R.D., Tuck, C.J., Ashcroft, I.A., 2018. Effective design and simulation of surface-based lattice structures featuring volume fraction and cell type grading. Mater. Des. 155, 220–232. https://doi.org/10.1016/j.matdes.2018.05.058.

Montazerian, H., Mohamed, M.G.A., Montazeri, M.M., Kheiri, S., Milani, A.S., Kim, K., Hoorfar, M., 2019. Permeability and mechanical properties of gradient porous PDMS scaffolds fabricated by 3D-printed sacrificial templates designed with minimal surfaces. Acta Biomater. 96, 149–160. https://doi.org/10.1016/j.actbio.2019.06.040.

Ruiz de Galarreta, S., Jeffers, J.R.T., Ghouse, S., 2020. A validated finite element analysis procedure for porous structures. Mater. Des. 189, 108546. https://doi.org/10.1016/j.matdes.2020.108546.

Wally, Z.J., Haque, A.M., Feteira, A., Claeyssens, F., Goodall, R., Reilly, G.C., 2019. Selective laser melting processed Ti6Al4V lattices with graded porosities for dental applications. J. Mech. Behav. Biomed. Mater. 90, 20–29. https://doi.org/10.1016/j.jmbbm.2018.08.047.

Wang, S., Liu, L., Li, K., Zhu, L., Chen, J., Hao, Y., 2019. Pore functionally graded Ti6Al4V scaffolds for bone tissue engineering application. Mater. Des. 168, 107643. https://doi.org/10.1016/j.matdes.2019.107643.

Xiong, Y.Z., Gao, R.N., Zhang, H., Dong, L.L., Li, J.T., Li, X., 2020. Rationally designed functionally graded porous Ti6Al4V scaffolds with high strength and toughness built via selective laser melting for load-bearing orthopedic applications. J. Mech. Behav. Biomed. Mater. 104, 103673. https://doi.org/10.1016/j.jmbbm.2020.103673.

Yang, L., Mertens, R., Ferrucci, M., Yan, C., Shi, Y., Yang, S., 2019. Continuous graded Gyroid cellular structures fabricated by selective laser melting: design, manufacturing and mechanical properties. Mater. Des. 162, 394–404. https://doi.org/10.1016/j.matdes.2018.12.007.

Zhang, X.Y., Fang, G., Leeflang, S., Zadpoor, A.A., Zhou, J., 2019. Topological design, permeability and mechanical behavior of additively manufactured functionally graded porous metallic biomaterials. Acta Biomater. 84, 437–452. https://doi.org/10.1016/j.actbio.2018.12.013.

Zhao, M., Zhang, D.Z., Liu, F., Li, Z., Ma, Z., Ren, Z., 2020. Mechanical and energy absorption characteristics of additively manufactured functionally graded sheet lattice structures with minimal surfaces. Int. J. Mech. Sci. 167 https://doi.org/10.1016/j.ijmecsci.2019.105262.

Zhou, H., Zhao, M., Ma, Z., Zhang, D.Z., Fu, G., 2020. Sheet and network based functionally graded lattice structures manufactured by selective laser melting: design, mechanical properties, and simulation. Int. J. Mech. Sci. 175 https://doi.org/10.1016/j.ijmecsci.2020.105480.